© [2008] IEEE. Reprinted, with permission, from Lu, Haiwei; Zhu, Jianguo; Lin, Zhi Wei (Jack); Guo, Youguang. 2008, 'A miniature short stroke linear actuator - Design and analysis', IEEE Transactions On Magnetics, Vol. 44, no. 4, pp. 497-504. This material is posted here with permission of the IEEE. Such permission of the IEEE does not in any way imply IEEE endorsement of any of the University of Technology, Sydney's products or services. Internal or personal use of this material is permitted. However, permission to reprint/republish this material for advertising or promotional purposes or for creating new collective works for resale or redistribution must be obtained from the IEEE by writing to pubs-permissions@ieee.org. By choosing to view this document, you agree to all provisions of the copyright laws protecting it.

A Miniature Short Stroke Linear Actuator: Design and Analysis

Haiwei Lu, Jianguo Zhu, *Senior Member, IEEE*, Zhiwei Lin, and Youguang Guo, *Senior Member, IEEE*

***Abstract*—Compared with the rotary-to-linear mechanism, linear actuators show advantages in terms of efficiency, thrust control, and system volume when linear motion is required. This paper presents the design and analysis of a newly developed miniature short stroke tubular linear permanent magnet actuator for robotic applications. The electromagnetic force of the actuator was optimized analytically by selecting appropriate dimensions. The force produced by the winding currents was then predicted by the finite element method under brushless DC excitation method. The actuation performance was also analyzed based on the dynamic modeling of the actuator. A prototype was constructed and tested on a specially designed test bench to verify the design. Moreover, the end effect on the magnetic force due to the limited length of the stator core and translator was analyzed and measured.**

***Index Terms*—Actuators, linear motors, tubular linear motors, permanent magnet motors, robotics.**

I. Introduction

ROBOTS IN FUTURE may have high intelligence and mobility but in a much smaller package. Miniature actuators are therefore the critical components to make these machines more dexterous, compact and cost effective [1]. The electric machine designers will thus face challenges raised by the downsized dimensions, such as simple structure, scaling effect, and micro-machining technology. Electromagnetic actuators are dominant in macro scale machines due to higher energy density and efficiency compared with their rivals, whereas for the miniature or micro scale applications, they were not favored because of the difficulties in fabrication and miniaturization of complicated electromagnetic structures. With the recent developments in nanomagnetic materials and micro machining technology, however, it is no longer difficult to extend them to miniature and even micro applications [2].

In general, actuators can be divided into two main categories according to their motion behavior: rotary and linear. In a system that requires linear motion, linear machines show advantages to the rotary-to-linear mechanisms in terms of efficiency, thrust control, and system volume [3]. In particular, linear actuators can greatly simplify the drive mechanism, which is crucial to the compactness of the systems. Moreover, application of new permanent magnet (PM) materials of high energy product and advanced control strategies can result in higher force-to-volume ratio and less cost of the machines [4].

Among various linear machine configurations, PM tubular machines have a number of distinctive features, such as high force density and excellent servo characteristics, which make them an attractive candidate for those applications in which dynamic performance and reliability are critical [5]. An application of PM tubular machines was described in [6], where the machine was developed for driving an experimental artificial heart pump. Another design for the similar purpose was reported in [7]. The proposed Φ70×20mm short stroke PM linear oscillatory actuator had only one stator winding and the tested maximum force is 63N under current of 1A. Other designs with different magnet topologies can be found in literature, such as radial, axial [8], and Halbach magnetized [9]. However, most of them were long stroke machines.

Studies were conducted over the past on the field analysis [5] [10] and design criteria [3] [11] of the tubular PM linear machines with different topologies. Most of them were accomplished based on analytical and/or numerical method and only one experimental prototype was presented based on the work [12]. For short stroke linear machines, some general design considerations were discussed in [13]. However, further analysis and experimental results of such kind of machines have not been found in literature.

This paper presents the design and analysis of a newly developed miniature short stroke PM tubular linear actuator for micro robotic actuations. The authors' aim is to develop such a machine whose overall size is less than one centimeter. Because the actuation force of an electromagnetic actuator will decrease dramatically due to the scaling effect [14], much concern should be taken on the performance of the electromagnetic force when the actuator is getting smaller. Additionally, high performance magnetic materials and simple configuration also need to be considered. In the paper, by applying advanced magnetic material, an analytical analysis was conducted to determine the appropriate dimensions of the

Manuscript received September 7, 2006, revised August 20, 2007..

Haiwei Lu is with the Faculty of Engineering, University of Technology, Sydney, NSW 2007, Australia (phone: +61-2-95142337; fax: +61-2-95142435; e-mail: haiwei@eng.uts.edu.au).

Jianguo Zhu is with the Faculty of Engineering, University of Technology, Sydney, NSW 2007, Australia (e-mail: joe@eng.uts.edu.au).

Zhi Wei Lin is with the Faculty of Engineering, University of Technology, Sydney, NSW 2007, Australia (e-mail: jacklin@eng.uts.edu.au).

Youguang Guo is with the Faculty of Engineering, University of Technology, Sydney, NSW 2007, Australia (e-mail: youguang@eng.uts.edu.au).

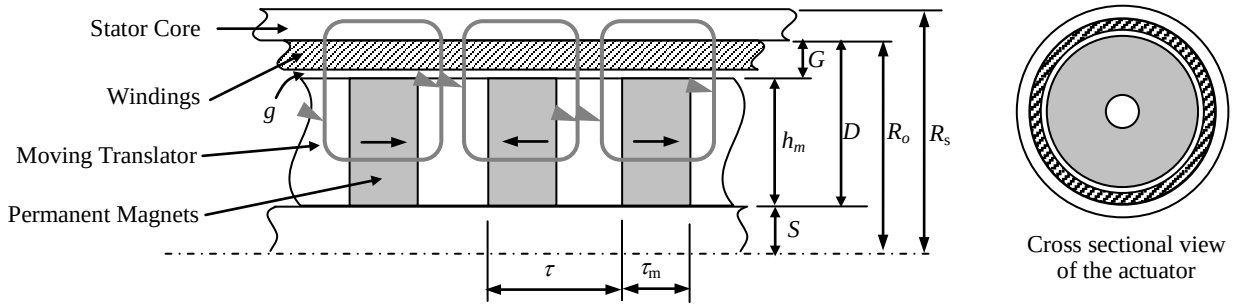

Fig. 1. Configuration of the slotless tubular PM actuator

actuator's key components for the optimal force output. The calculation was numerically verified by the finite element (FE) magnetic field analysis. According to the proposed application, the electromagnetic force of the actuator produced by brushless DC drive method was then predicted by the FE solutions and the results were experimentally tested for verification. The reluctance force caused by the finite length of the stator core was also analyzed and tested. Moreover, the operational performance of the designed actuator was analyzed based on the magnetic analysis and dynamic modeling.

TABLE I
DIMENSIONS OF THE ACTUATOR UNIT: mm

Stator Outer Radius (R_e)	16
Stator Inner Radius (R_o)	13.75
Stator Length (L_s)	34
Air Gap (g)	0.4
Translator Radius (h_m+S)	11.25
Translator Length (L_a)	20
Shaft Radius (S)	2.5

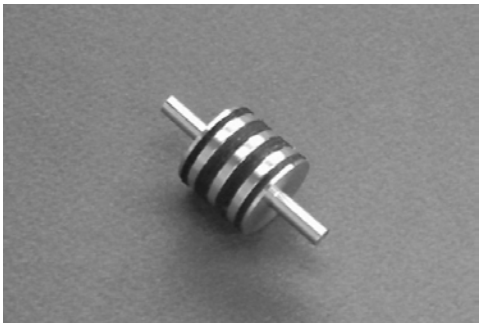

(a) Assembly of the moving translator

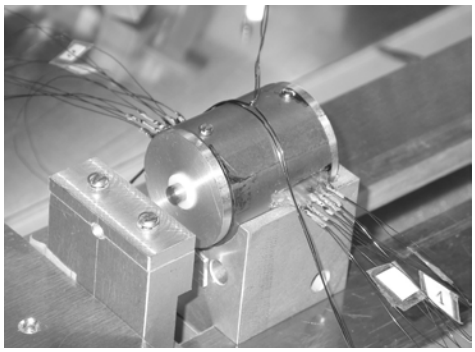

(b) Completed prototype of the actuator

Fig. 2. The proposed linear PM actuator

II. ACTUATOR DESIGN

A. Basic Structure

Fig. 1 illustrates the basic configuration of the proposed tubular linear interior-mounted PM actuator. Table I lists the elementary dimensions of the first testing prototype. The stroke length was designed as 6mm. The tubular stator core is made up of the glassy metal ribbon, which is an amorphous soft magnetic material with high magnetic permeability and extremely low core loss. Its saturation induction is 1.56T and the maximum relative DC permeability can reach 45000. The core loss of the material is typically less than 0.2W/kg at 60Hz/1.4T. Circular concentrated phase windings are mounted inside the stator core. Due to the small stator diameter, the slotless structure is employed for the simplicity in construction. Moreover, the slotless windings can also result in a better dynamic performance and less cogging force [3] [5]. The coils used for constructing the phase windings are made of 0.2mm copper wire with 70 turns.

The PMs used in the translator are NdFeB discs and the pole-pieces between the magnets are also made by the glassy metal ribbon. The shaft supporting the magnets and pole-pieces on the translator is made of non-ferromagnetic material for the reduction of the entire effective air gap between the stator core and translator, the volume of the PM material and the moving mass [5]. The translator is stacked by putting the magnets and the pole-pieces alternately along the shaft, as shown in Fig. 2(a), and the completed prototype of the actuator is shown in Fig. 2(b). The number of magnets on the translator is determined according to the desired length of the actuator and the tradeoff between the flux density and the saturation of the magnetic core [13].

B. Design for Optimal Force Output

According to Lenz's law, the force produced by a current i interacting with a magnetic field B can be expressed as

$$F = i\vec{L}_c \times \vec{B}\,, \tag{1}$$

where L_c is the length of the conductor exposed to the magnetic field. Based on the basic configuration of the proposed actuator shown in Fig. 3, it can be derived that the electromagnetic force of the phase coils under one pole, F_{emp}, is

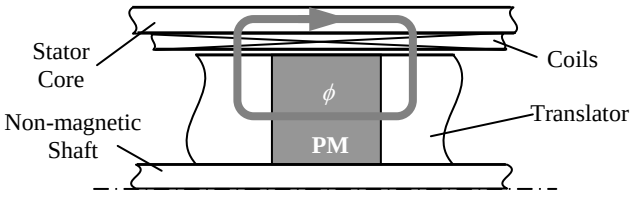

Fig. 3. Magnetic flux under a pair of poles

$$F_{emp} = \int_0^{d_c} B_{gr}(x) J_s h_c l_c dx, \quad (2)$$

where $B_{gr}(x)$ is the radial component of the flux density in the air gap, J_s the current density in the coil, and h_c, d_c and l_c are the height, effective width and mean perimeter of the coils under one pole, respectively. The integration $\int_0^{d_c} B_{gr}(x)dx$ gives the magnetic flux per pole, ϕ_{gr}. Because the phase coils are concentrated, the current density J_s is constant at a given time instant. As a result, (2) can be rewritten as

$$F_{emp} = \phi_{gr} J_s h_c l_c . \quad (3)$$

It can be seen that the force per pole is proportional to the magnetic flux per pole and the dimensions of the coil. Hence, an optimal force output can be achieved by suitable design of ϕ_{gr} and inner diameter of the actuator that makes the best utilization of the actuator volume.

In order to simplify the ongoing analysis, the following assumptions are made:

(i) The magnetic permeability of magnetic core is regarded as infinite;

(ii) The leakage flux in the air gap and shaft is ignored; and

(iii) The flux produced by the winding currents is negligible compared with the flux produced by the PMs.

1) Flux under one pole

The magnetic flux under one pole produced by the PMs can be found as [15]

$$\phi_{gr} = \frac{\mu_0 \pi H_c \tau_m}{4G/\left((2h_m + 2S + G)(\tau - \tau_m)\right) + \tau_m / \left(h_m (h_m + 2S)\right)}, \quad (4)$$

where H_c is the coercive force of the PMs, τ the pole pitch of the translator, τ_m the width of the PM disc, h_m the radial depth of the PM disc, G the gap between the stator and translator, and S the radius of the non-ferromagnetic shaft.

Under the conditions of fixed outer dimensions and number of poles, say, taking h_m, G and τ as constants, the flux and flux density in the air gap will vary with the width τ_m of the PMs and there exists a maximum flux at a certain width of PMs. By eliminating τ_m in the numerator in (4), the following can be yielded,

$$\phi_{gr} = \frac{\mu_0 \pi H_c}{4G/\left((2h_m + 2S + G)(\tau\tau_m - \tau_m^2)\right) + 1/\left(h_m (h_m + 2S)\right)}. \quad (5)$$

Based on (5), the variation of the flux and flux density under one pole are obtained and shown in Fig. 4. It can be easily found that the magnetic flux per pole will reach the maximum when $\tau_m = \tau/2$.

2) Force per pole

The electromagnetic force per pole can be found by combining (3) and (5). By applying $\tau_m = \tau/2$, the force per pole will be obtained as

$$F_{emp} = \mu_0 \pi H_c J_s k_f \frac{\tau^2 h_m (D - h_m)(2S + h_m)(D + 2S + h_m)}{16 h_m (D - h_m)(2S + h_m) + \tau^2 (D + 2S + h_m)}, \quad (6)$$

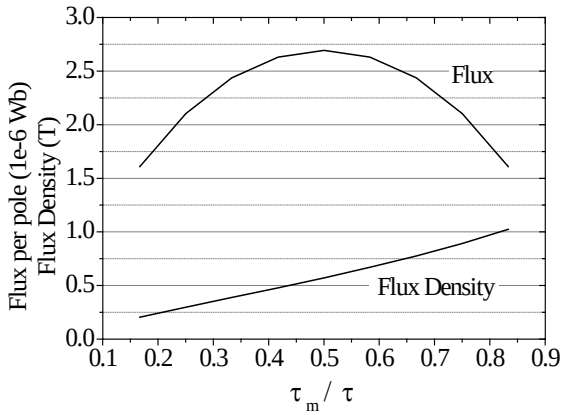

Fig. 4. Variation of flux and flux density vs. τ_m/τ

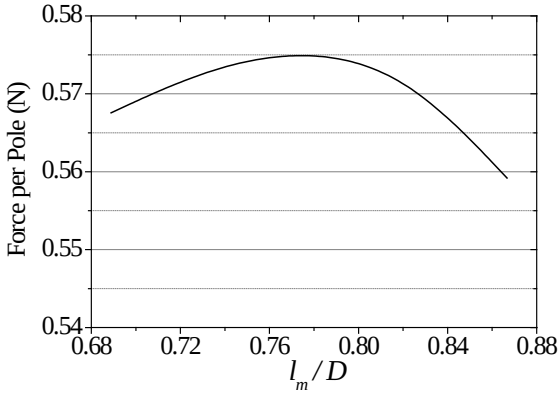

Fig. 5. Electromagnetic force per pole vs. l_m/D by analytical method

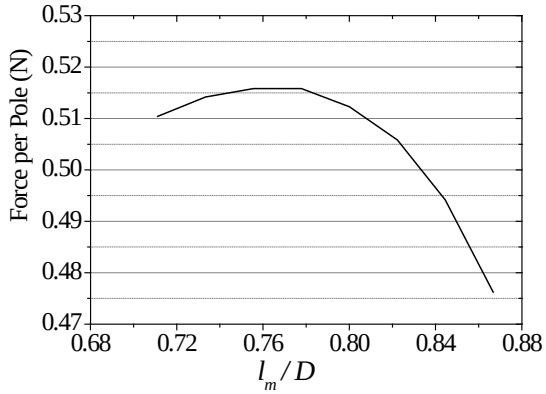

Fig. 6. Electromagnetic force vs. l_m/D by the FE analysis

where k_f is the fill factor of the windings, and $D = G + h_m$ the gap between the stator core and the shaft, as shown in Fig. 1.

It is seen from (6) that, if the distance between the stator core and translator shaft is fixed. In other words, the gap D is constant, and the force per pole will be a function of l_m, or the height of the coils, h_c. For the dimensions listed in Table I, the variation of the force per pole versus the ratio of l_m/D is plotted in Fig. 5. It can be seen that there also exists an optimal ratio of l_m/D to achieve a maximum force or force-to-volume ratio. From the formulation, it can be found that the optimal ratio of l_m/D is around 0.78 and the maximum force per pole is 0.58N when the current density of coils J_s is set as $6\text{A}\cdot\text{mm}^{-2}$, the thermal tether of copper wire under given conditions.

Numerical method was applied to verify the above analytical results. By performing a two-dimensional (2D) non-linear FE analysis of the actuator, the flux density in the air gap and the electromagnetic forces produced in the stator windings were computed. The saturation effect of the magnetic core was taken into account during the analysis. The effective flux density in the air gap was found to be around 0.51T and the total electromagnetic force was calculated at different l_m/D ratios as shown in Fig. 6. It is shown that the analytical results agree well with the numerical results.

III. Flux Density and Electromagnetic Force

Since the translator of the actuator is deliberately designed shorter than the stator so that it can move back and forth within the stator, the distribution of the resultant flux density within the stator windings varies with the position of the translator. Consequently, the produced electromagnetic force also varies. Moreover, due to the limited length of the actuator, the flux density and force when the translator is close to the ends of the stator core will differ from those when the translator is in the middle of the actuator.

In order to find out the detailed flux density distribution and the profile of the electromagnetic force of the actuator, an FE model considering the non-linear properties of the magnetic core was established according to the above analysis. Meanwhile, several factors related to the construction of the prototype were also considered during modeling, such as the lamination factor of the magnetic core, the tolerances required for the machining and installation, etc. Fig. 7 shows the magnetic flux contour plot when the translator is at two different positions: (a) in the middle, and (b) at the right end of the actuator.

A. Flux Density in Stator Windings

The stator windings consist of twelve coils. Because the stator windings are concentrated, each phase coil occupies a part of the air gap, and the distribution of the phase winding is arranged as *A-C-B-…-B*. Accordingly, the flux density within the stator windings was analyzed based on the coils and grouped by phases. The flux density in each of the coils was computed at different translator positions and the results are plotted in Fig. 8, where the corresponding phase and coil numbers are indicated in Fig. 7. The flux generated by the winding currents was also considered during the computation. Nevertheless, the flux produced by the currents is considerably small compared to the flux generated by the PMs and will make no changes to the profiles of the flux densities within the stator windings.

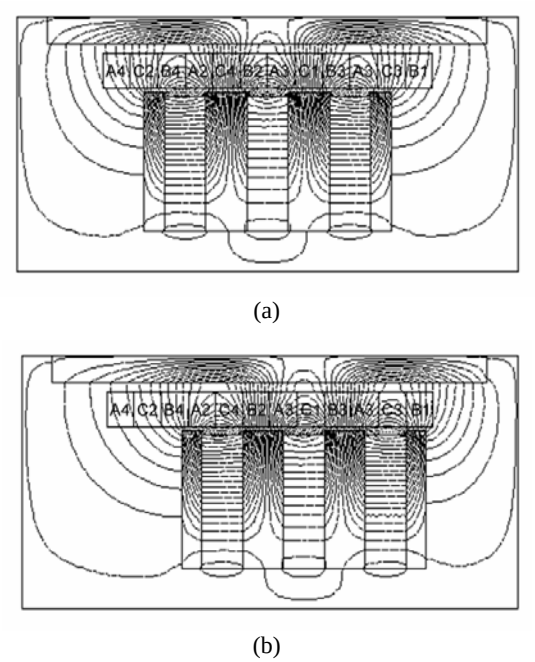

Fig. 7. 2D flux contour plots when the translator is (a) in the middle, and (b) at the right end of the actuator

From the results, it is shown that the variation of the flux density within the windings is close to sinusoidal waveform. However, the end effect is remarkable when the translator is close to the stator ends, especially for those coils near to the ends of the actuator, such as the 4th coil in phase A, the 1st coil in phase B and the 2nd and 3rd coils in phase C. The flux densities in these coils no longer vary as sinusoidal and are much smaller than others.

The information of these flux densities can be very useful in the circuit model of the actuator. In the commonly used rotary machines, the back electromotive force (EMF) can be obtained simply by the fundamental component of the flux density in the stator windings. The flux densities in the short stroke linear actuator, however, show very strong non-linearity and distortion and the conventional method of using only the fundamental component of the flux density would lead to significant errors when computing the back EMF. Hence, the actually obtained flux density profiles should be used directly for predicting the back EMF in the phase windings at different translator positions in the dynamic model of the actuator.

B. Electromagnetic Force under Brushless DC Excitation

Based on the obtained flux densities in the windings, the electromagnetic force can be calculated by using (1). Considering the proposed application of the designed actuator, a simple but effective drive method should be adopted. The brushless DC drives are widely used in the PM machine applications due to their simple implementation and very good

control performance. Moreover, the brushless DC drive without the mechanical position sensor can also be easily realized by phase voltage detection. These features are very attractive for the miniature systems that do not allow complex system configuration and large volume.

The excitations of the linear brushless DC drive are direct currents imposed to the phase windings according to the translator positions of the linear PM machine. The phase currents are required to be commutated at specific translator positions to achieve the optimal force output. Ideally, the peak torque occurs when the fields of stator and translator are at 90° to each other and falls off as the fields move together. In order to keep the machine running, the magnetic field produced by the stator windings should shift position as the translator moves to catch up with the stator field. As a result, it is important to know the translator position to determine which windings shall be energized following the energizing sequence. Usually, the translator position is sensed by using mechanical position sensors installed on the machine stator. However, the employment of mechanical position sensors results in a higher drive cost due to sensors, wiring and implementation in the machine. Moreover, physical sensors cannot be used in those applications where space is extremely restricted, such as micro robotics. Therefore, the sensorless drive is an essential capability of a brushless DC machine drive.

During the FE force analysis, the electromagnetic force of the actuator was computed at different translator positions with a pre-defined excitation pattern. Since the conventional 120˚ square wave of energization (Fig. 9) is applied for the current commutation of the actuator drive, a proper switching sequence as well as a set of commutation positions can be found by comparing the produced forces under different commutation schemes. Table II lists the obtained switching sequence and the corresponding commutation positions throughout the entire stroke and Fig. 10 shows the computed electromagnetic force by applying the sequence. In the

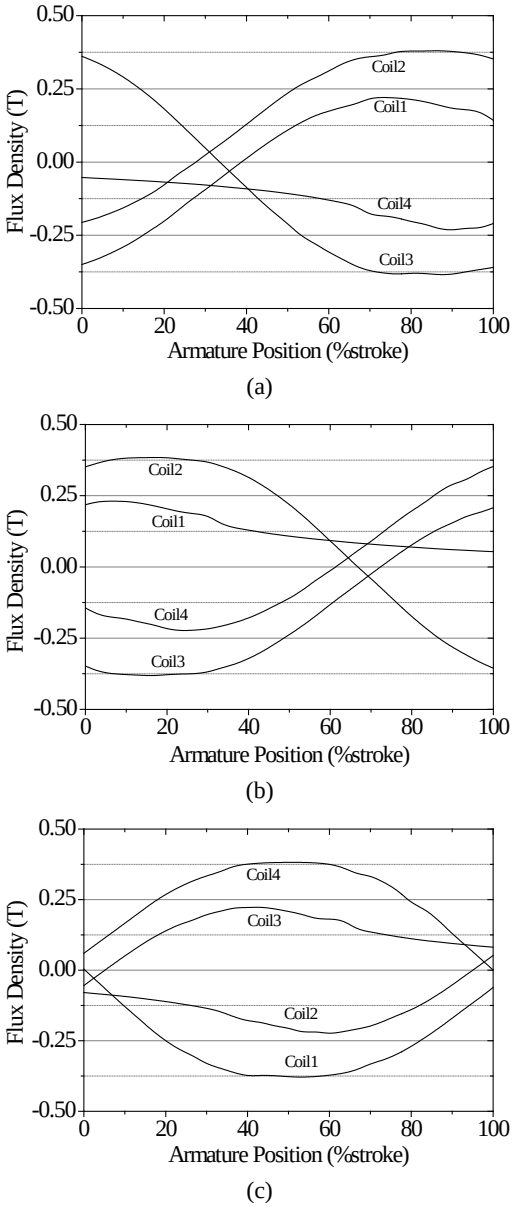

Fig. 8. Flux densities in each phase coils at different translator positions (a) phase A, (b) phase B, (c) phase C

TABLE II
Energization Sequence

Stroke	0 – 13.3%	13.3 – 50%	50 – 86.7%	86.7 – 100%
Energization Sequence	$A\overline{B}$	$\overline{B}C$	$\overline{A}C$	$\overline{A}B$

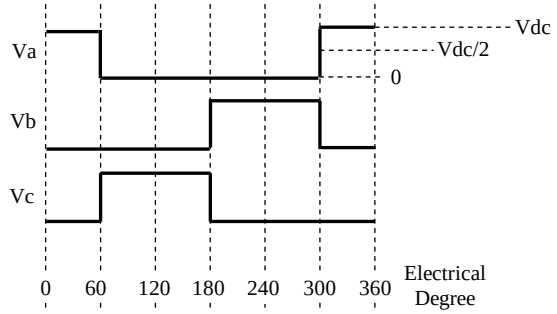

Fig. 9. Conventional 120˚ energization

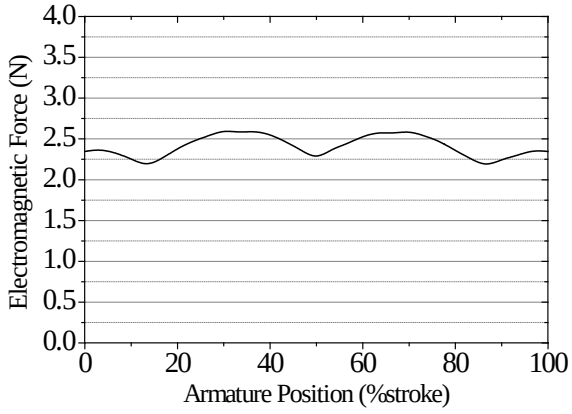

Fig. 10. Predicted electromagnetic force under brushless DC excitation

calculation, the phase currents are set to meet the current density limitation of $6A \cdot mm^{-2}$ as used in the machine design.

As common in the brushless DC drives, the output force of the actuator has ripples due to the DC phase currents and the current commutation. The influence of the end effect on the electromagnetic force can also be clearly seen from the results. Although the force obtained by the brushless DC drive method is usually less than that produced by the three-phase energized scheme, its control method is much simpler and can be easily realized by less hardware compared to the three phase drive method. This feature is preferable for the compact systems, especially micro systems. Moreover, the sensorless control can be readily implemented in the brushless DC drive method by detecting the back EMF in the unexcited phase of the machine. This attribute is also essential for the miniature or micro applications that the installation of mechanical position sensors is unfeasible.

IV. Experiment on Prototype

A comprehensive experiment was carried out on the prototype to verify the previous analysis and the performance of the proposed actuator.

A precision test bench was implemented for the static testing of the prototype. The test bench consists of a force gauge, a micro position meter, a set of tools for clamping the actuator tested, and a supporting stage, as shown in Fig. 11. In order to measure the static force generated by the actuator at different translator positions, the position of the translator was preset by the micrometer before the measurement. The polarity of the stator current was applied to make the force against the force gauge so that the force can be effectively sensed. Much care should be taken with the static friction between the linear bearings and the shaft of the translator of the actuator while testing. The friction should be reduced as much as possible to obtain better results.

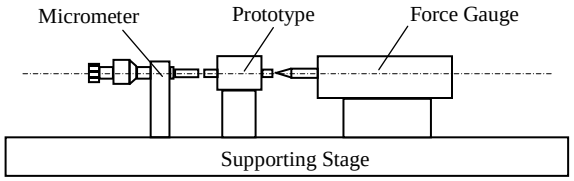

(a) Configuration

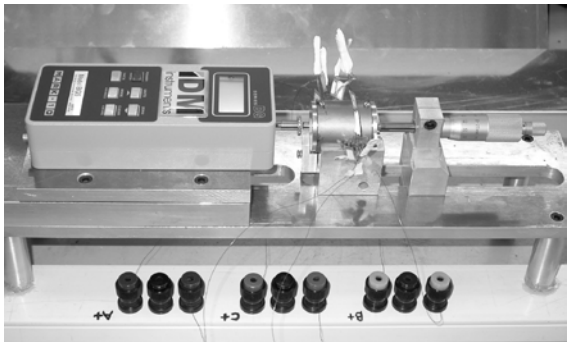

(b) Implementation

Fig. 11. Test bench for the prototype verification

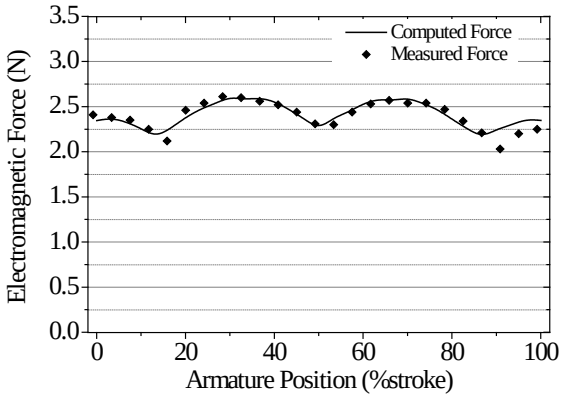

Fig. 12. Electromagnetic force under brushless DC excitation

The proper energized phases and currents direction imposed to the actuator were set according to the preset translator positions and the energization sequence shown in Table II. The amplitude of the current was set to 220mA to meet the current density used for the force prediction. Totally 25 positions were tested throughout the entire stroke of the actuator. The measured output force is plotted together with the predicted results in Fig. 12 as a comparison. It can be seen that the predicted forces agree well with the measurement results.

V. Reluctance Force due to End Effect

Although the slotless structure eliminates the cogging force due to the interaction between the core teeth and the magnets, there still exists another reluctance force within the linear actuator due to the limited length of the stator core and moving translator. Similar to the slot structure in an electrical machine, the short stroke actuator can be considered as one tooth pair between the translator and stator, as shown in Fig. 13. A reluctance force will result from the variation of the magnetic reluctance between the stator core and the moving translator, and the force will lead to the alignment of the stator core and the translator with their center positions.

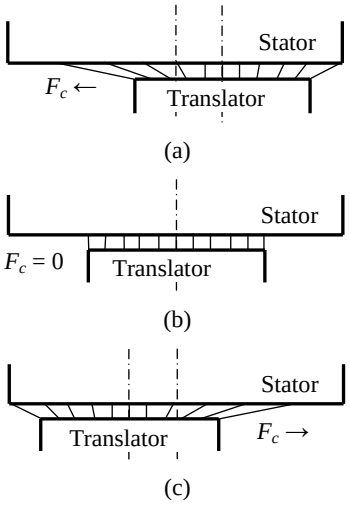

Fig. 13. Reluctance force when translator is at (a) Right, (b) Center, and (c) Left

The resultant reluctance force can be predicted by numerical solutions based on the virtual work or Maxwell tensor method. The FE method can provide good results in magnetic field analysis. However, a considerable care is required with the mesh discretization to achieve high computational accuracy in force analysis [16]. The predicted results of the reluctance force at different translator positions by using FE analysis are shown in Fig. 14 combined with a comparison of the computational accuracy under different meshing scales. Because the reluctance force will be zero when the translator is centered within the stator core, it is used as an indicator for the accuracy in the plot. The *Nesize* used in the plot is the normalized element size while the base element size is the one used for the last results.

The reluctance force of the proposed actuator was also measured by using the test bench and the results are plotted in Fig. 14 as well. It can be seen that the predicted values are larger than those from the measurement. This could be attributed to the larger fringing flux in the practical prototype than that in the numerical model.

The force could affect the entire dynamic performance of the actuator. In some particular applications, the force may be useful. For example, if the actuator is used as an impact drive, this reluctance force could help to restore the translator position and to alleviate the impact force when collision occurs between the stator and translator.

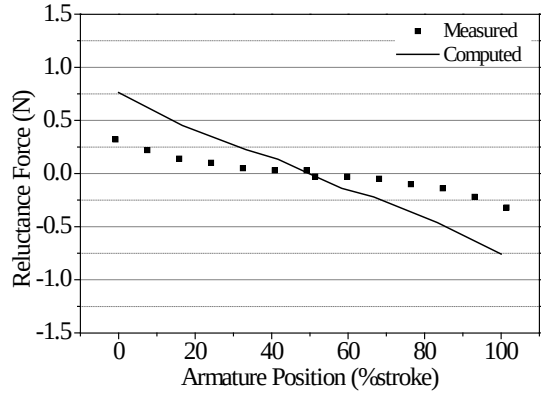

(a) Reluctance force

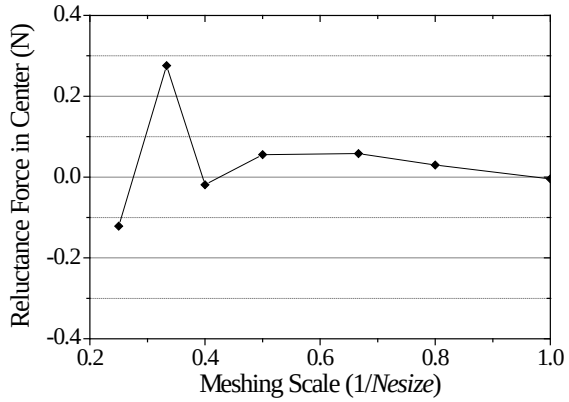

(b) Comparison of computational accuracy under different meshing scales

Fig. 14. Analysis of reluctance force caused by end effect

VI. Dynamic Modeling and Analysis

A dynamic model is essential for analyzing the performance of an electric machine. The previous electromagnetic field analysis of the designed actuator provides the basic information of the machine for establishing a system model.

A. Dynamic model

Through the analysis of the flux linkage in each phase, electro-dynamic equations of the designed actuator can be obtained as follows

$$u_j = R_j i_j + L_{jj}\frac{di_j}{dt} + L_{jk}\frac{di_k}{dt} + L_{jl}\frac{di_l}{dt} + e_{jm} \tag{7}$$

where u_j, i_j, R_j, L_{jj}, and e_{jm} are voltage, current, resistance, self-inductance, and back EMF in phase j, L_{jk} and L_{jl} are the mutual inductances between phases, and $j, k, l \in (a, b, c)$, $j \neq k \neq l$. The back EMF in each phase can be further expressed as

$$e_{jm} = 2\pi r_c N B_{jr} v_a \tag{8}$$

where r_c and N are the mean radius and number of turns of the phase coils, v_a is the translator velocity with respect to the stator, and B_{jr} the radial component of the flux density in each phase, which can be derived by the corresponding flux densities in each of the phase coils [17].

The dynamic force of the actuator can be found by the derivative of the corresponding system co-energy with respect to the displacement, i.e. $F_{em}=\partial W_f'/\partial z$, and it is given by

$$F_{em} = 2\pi r_c N(B_{ar} i_a + B_{br} i_b + B_{cr} i_c) \tag{9}$$

B. Performance Analysis

Based on the above equations, combined with the kinetic equation of the actuator, one can form the dynamic model of the designed actuator. A SIMULINK model is hence established as shown in Fig. 15 and can be readily employed to analyze the dynamic performance of the actuator.

Fig. 16 shows the analyzed dynamic performances during one stroke when the actuator is driven by brushless DC method. The external load force was set as 2.4N, which is close to the maximum force capability of the actuator. As previously mentioned, the brushless DC drive of the actuator could only operate based on the proper translator positions, and a physical linear position feedback was therefore assumed in the analysis. This, however, could be impractical in the miniature or micro applications and a kind of sensorless control scheme should be adopted, such as back EMF sensing technique. Moreover, senorless startup of the system should also be considered and preset of the initial translator position by mechanical or electrical method could be the solutions in specific applications. Some initial position detection by finding the saliency effect of the machine can be employed in those applications that require high driving performance.

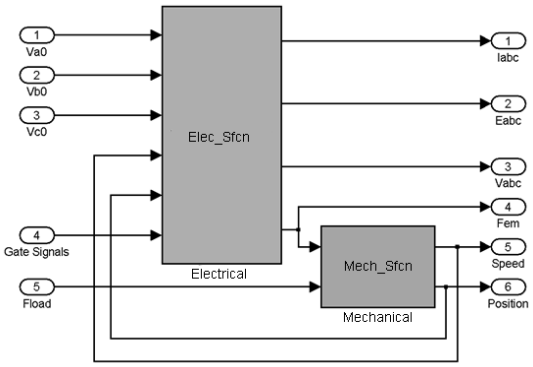

Fig. 15. SIMULINK model of the tubular PM actuator

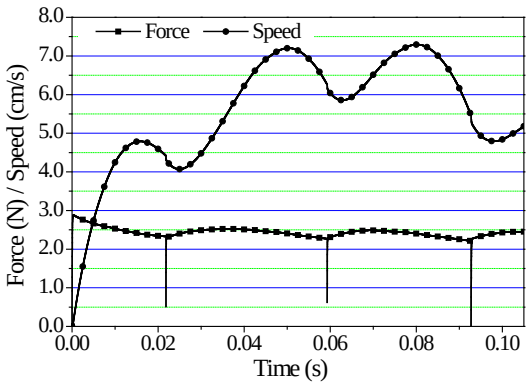

Fig. 16. Analyzed dynamic performance with brushless DC drive

VII. Conclusion

The design and analysis of a newly developed tubular interior-mounted PM linear actuator is presented in this paper. By using both the analytical and numerical methods, the key dimensions of the actuator were determined through the optimization of the electromagnetic force. Via the FE analysis, the flux density and electromagnetic force at different translator positions were predicted. The computed results were compared with the experimental results obtained from a prototype and the validity of the design was confirmed by the experiment. In addition, the dynamic actuation performance of the linear actuator was analyzed based on the system modeling. The results show that the designed tubular PM actuator could be suitable for a practical miniature robotic system.

References

[1] A. M. Flynn, L. S. Tavrow, S. F. Bart, R. A. Brooks, D. J. Ehrlich, K. R. Udayakumar, and L. E. Cross, "Piezoelectric micromotors for microrobots," *Journal of Microelectro-mechanical Systems*, vol. 1, no. 1, pp. 44-51, Mar. 1992.

[2] Haiwei Lu and Jianguo Zhu, "A comparison of piezoelectric and mlectromagnetic microactuators," *JSAEM Studies in Applied Electromagnetic and Mechanics*, vol. 15, pp. 101-107, 2005.

[3] N. Bianchi, S. Bolognani, and F. Tonel, "Design consideration for a tubular linear PM servo motor," *EPE Journal*, vol. 11, no. 3, pp. 41-47, Aug. 2001.

[4] Haiwei Lu, Jianguo Zhu, and Youguang Guo, "A tubular linear motor for micro robotic applications," in *Proc. IEEE 2005 Int. Conf. on Mechatronics*, Taipei, Taiwan July 10-12, 2005, pp. 596-601.

[5] Jiabin Wang, G. W. Jewell, and D. Howe, "A general framework for the analysis and design of tubular linear permanent magnet machines," *IEEE Trans. Magn*., vol. 35, no. 3, pp. 1986-2000, May 1999.

[6] J. J. Cathey, D. A. Topmiller, and S. A. Nasar, "A tubular self-synchronous motor for artificial heart pump drive," *IEEE Trans. Biomed. Eng.*, vol. 33, no. 3, pp. 315-319, Mar. 1986.

[7] D. Ebihara and M. Watada, "Development of single winding Linear Oscillatory Actuator," *IEEE Trans. Magn.*, vol. 28, no. 5, pp. 3030-3023, Sept. 1992

[8] Z. Q. Zhu, P. J. Hor, D. Howe, and J. Rees-Jones, "Novel linear tubular brushless permanent magnet motor," *in Proc. IEEE 8th Int. Conf. on Electrical Machines and Drives*, Cambridge, MA, USA, Sept. 1-3 , 1997, pp. 91-95

[9] Seok Myeong Jang, Jang Young Choi, Sung Ho Lee, Sung Kook Cho, and Won Bum Jang, "Analysis of the tubular motor with Halbach and radial magnet array," *in Proc. IEEE 6th Int. Conf. on Electrical Machines and Systems*, vol. 1, Nov. 9-11, 2003, Beijing, China, pp. 250-252

[10] Jiabin Wang, D. Howe, and G. W. Jewell, "Analysis and design optimization of an improved axially magnetized tubular permanent-magnet machine," *IEEE Trans. Energy Conversion*, vol. 19, no. 2, pp. 289-295, June 2004.

[11] N. Bianchi, S. Bolognani, and F. Tonel, "Design criteria of a tubular linear IPM motor," *in Proc. IEEE 2001 Int. Electric Machines and Drives Conf.*, Cambridge, MA, USA, June 17-20, 2001, pp. 1-7.

[12] N. Bianchi, S. Bolognani, D. D. Corte, and F. Tonel, "Tubular linear permanent magnet motors: an overall comparison," *IEEE Trans. Ind. Applicat.*, vol. 39, no. 2, pp. 466-475, March-April 2003.

[13] B. Lequesne, "Permanent magnet linear motors for short strokes," *IEEE Trans. Ind. Applicat*., vol. 32, no. 1, pp. 161-168, Jan.-Feb. 1996.

[14] Haiwei Lu and Jianguo Zhu; "A comparative study of microactuators driven by electric and magnetic principles," in *Proc. Australasian Universities Power Engineering Conference*, Brisbane, Australia, Sept. 26-29, 2004, paper ID.79.

[15] Haiwei Lu, Jianguo Zhu, and Youguang Guo, "Development of a slotless tubular linear interior permanent magnet micro motor for robotic applications," *IEEE Trans. Magn.*, vol. 41, no. 10, pp. 3988-3990, Oct. 2005.

[16] D. Howe and Z. Q. Zhu, "The influence of finite element discretization on the prediction of cogging torque in permanent magnet excited motors", *IEEE Trans. Magn*., vol. 28, no. 2, pp.1080-1083, Mar. 1992.

[17] Haiwei Lu, Jianguo Zhu, and Youguang Guo, "A permanent magnet linear motor for micro robots," *in Proc. IEEE International Conference on Power Electronics and Drive Systems*, vol. 1, Nov. 28 - Dec. 1, 2005, Kuala Lumpur, Malaysia, pp. 590-595

Haiwei Lu received the B.E. and M.E. degrees in electrical engineering from Tsinghua University, Beijing, China, in 1991 and 1993, respectively.

From 1993 to 2003, he was a lecturer in the Power Electronics and Electrical Machine Division, Department of Electrical Engineering, Tsinghua University, Beijing, China. He is currently a PhD student in the Faculty of Engineering, University of Technology, Sydney. His research interests are power electronics and the design and control of electrical machines.

Jian Guo Zhu (SM'03) received the B.E and M.E. degrees in China from Jiangsu Institute of Technology in 1982 and Shanghai University of Technology in 1987, respectively, and the Ph.D degree from University of Technology, Sydney (UTS), Australia, in 1995.

He is currently the Professor of Electrical Engineering at UTS. His research interests are electromagnetics and electrical machines and drives.

Zhi Wei Lin received the Ph.D Degree in physics from the University of New South Wales, Sydney, Australia in 2000.

He joined University of Technology, Sydney as a research fellow in 2002. His research interests include electromagnetic properties in superconducting materials, colossal magnetoresistive materials, coarse and nanostructured soft magnetic materials using magneto-optical imaging and three-dimensional magnetic property measurement system.

Youguang Guo (S'02-M'05-SM'06) received the B.E. degree from Huazhong University of Science and Technology (HUST), China in 1985, the M.E. degree from Zhejiang University, China in 1988, and the PhD degree

from University of Technology, Sydney (UTS), Australia in 2004, all in electrical engineering.

From 1988 to 1998, he was an associate lecturer/lecturer in the Department of Electrical Engineering, HUST. From March 1998 to July 2000, He was a visiting research fellow in the Center for Electrical Machines and Power Electronics, Faculty of Engineering, UTS.

Dr. Guo is currently an ARC (Australia Research Council) postdoctoral research fellow at UTS. His research fields include modeling of magnetic properties of magnetic materials, numerical analysis of electromagnetic field, motor design and optimization, power electronics and control of electrical appliance. He has published over 150 refereed technical papers including 77 journal articles.